Crystal structure of DNA-bound Co(III)·bleomycin B_2: Insights on intercalation and minor groove binding

Kristie D. Goodwin*, Mark A. Lewis†, Eric C. Long†‡, and Millie M. Georgiadis*†‡

*Department of Biochemistry and Molecular Biology, Indiana University School of Medicine and †Department of Chemistry and Chemical Biology, Purdue School of Science, Indiana University–Purdue University Indianapolis, Indianapolis, IN 46202

Edited by Douglas C. Rees, California Institute of Technology, Pasadena, CA, and approved February 8, 2008 (received for review August 28, 2007)

Bleomycins constitute a widely studied class of complex DNA cleaving natural products that are used to treat various cancers. Since their first isolation, the bleomycins have provided a paradigm for the development and discovery of additional DNA-cleaving chemotherapeutic agents. The bleomycins consist of a disaccharide-modified metal-binding domain connected to a bithiazole/C-terminal tail via a methylvalerate-Thr linker and induce DNA damage after oxygen activation through site-selective cleavage of duplex DNA at 5′-GT/C sites. Here, we present crystal structures of two different 5′-GT containing oligonucleotides in both the presence and absence of bound Co(III)·bleomycin B_2. Several findings from our studies impact the current view of bleomycin binding to DNA. First, we report that the bithiazole intercalates in two distinct modes and can do so independently of well ordered minor groove binding of the metal binding/disaccharide domains. Second, the Co(III)-coordinating equatorial ligands in our structure include the imidazole, histidine amide, pyrimidine N1, and the secondary amine of the β aminoalanine, whereas the primary amine acts as an axial ligand. Third, minor groove binding of Co(III)·bleomycin involves direct hydrogen bonding interactions of the metal binding domain and disaccharide with the DNA. Finally, modeling of a hydroperoxide ligand coordinated to Co(III) suggests that it is ideally positioned for initiation of C4′-H abstraction.

antitumor | DNA-binding | HOO-Co(III) bleomycin

The bleomycins are a family of glycopeptide-derived antitumor natural products first isolated from *Streptomyces verticillus* by Umezawa (1). Bleomycins are used to treat lymphomas (2, 3) and testicular cancers (4), most often in combination therapies. The clinical efficacy of the bleomycins is thought to derive from their ability to mediate single- and double-strand DNA cleavage (5, 6) resulting from Fe^{2+} and O_2-dependent (7) C4′-H abstraction from pyrimidine nucleotides (8) contained within 5′-GT/C dinucleotide sites (9). Of the DNA lesions formed, double-strand DNA cleavage is thought to be most relevant to the cytotoxicity of bleomycin. Although DNA is the generally accepted locus of drug activity, O_2-activated Fe(II)·bleomycin also mediates the selective cleavage of RNA (10), and Cu(I)·bleomycin is capable of cleaving DNA (11); however, the *in vivo* relevance of this alternative nucleic acid target and metal ion remain to be fully determined.

The metallobleomycins have served as an important paradigm for nucleic acid-targeted drug design (12, 13); and yet, despite extensive study over the past 40 years, fundamental aspects of their activity have yet to be fully defined including the role of particular DNA-binding modes on drug activity and the mechanism of double-strand DNA cleavage (14). Facilitating structural studies, HOO-Co(III)·bleomycin "green" (Fig. 1) (15) constitutes a stable structural analogue of O_2 activated Fe(II)·bleomycin, HOO-Fe(III)·bleomycin, that interacts with the same DNA site-selectivity (16–20) but requires photoactivation to cleave DNA. From 2D NMR derived models reported for DNA-bound HOO-Co(III)·bleomycin, the bithiazole is intercalated and the pyrimidinyl ring of the metal-binding domain interacts with the guanine of the 5′-GC site via the minor groove (21–25). Although these studies have provided key information, the impact of drug binding on the substrate DNA structure has not been fully addressed. Here, we present the crystal structures of duplex DNA-bound HOO-Co(III)·bleomycin B_2 (Co·BLM) determined at 2.8 Å and 2.3 Å (PDB ID codes 2R2S and 2R2U), respectively, for DNA sequences **1** and **2** (Fig. 1). We also describe the structures of these same duplex DNAs in the absence of bound drug at 2.1 and 2.0 Å (PDB ID codes 2R2R and 2R2T) and discuss implications for recognition and cleavage of DNA by metallobleomycin.

Results

Description of the Structures. Crystal structures of Co·BLM bound to DNA were determined by using a host-guest system (26–29) in which the N-terminal fragment of Moloney murine leukemia virus reverse transcriptase (RT), the "host," is bound to the termini of d(ATTA**GT**TATAACTAAT)$_2$ (**1**) or d(ATTTA**GT**-TAACTAAAT)$_2$ (**2**), each containing two preferred sites of drug binding, as the "guests" (Fig. 1). The desired complexes were obtained through soaking Co·BLM (Fig. 1) into preformed RT-DNA crystals. Binding of Co·BLM was found to correlate with a change in the unit cell dimensions compared with unbound RT-DNA crystals [supporting information (SI) *Text* and Table S1]. No change in crystal color was observed after exposure to X-rays suggesting that the hydroperoxide ligand remained intact.

Of the two complexes, **1** displayed ordered density for the entire Co·BLM molecule excluding the hydroperoxide ligand and the propionamide, whereas **2** only exhibited ordered density for the intercalated bithiazole and a portion of the C-terminal tail. Co·BLM was found to occupy a 5-bp site in **1** including residues G_5 through T_7 and A_{10} through A_{14} on the complementary strand (Figs. 1 and 2). The asymmetric unit of the RT-DNA crystals contains one molecule of the protein and 8 bp of the DNA before Co·BLM binding. After Co·BLM intercalation, the asymmetric unit for the drug complex includes one protein molecule, one Co·BLM, and 7.5 bp. To accommodate the intercalation of Co·BLM, which occupies the space of 1 bp, the adenines of the two A-T base pairs flanking the dyad are extruded, and a T-T base pair results (Figs. 1–3). This rearrangement at the dyad may be facilitated by breathing of A-T base pairs (30) and does not impact drug-DNA binding. The expected Co·BLM-induced changes in rise, helical twist, and minor groove

Author contributions: K.D.G., E.C.L., and M.M.G. designed research; K.D.G., M.A.L., and M.M.G. performed research; K.D.G. and M.M.G. analyzed data; and K.D.G., E.C.L., and M.M.G. wrote the paper.

The authors declare no conflict of interest.

This article is a PNAS Direct Submission.

Data deposition: The atomic coordinates have been deposited in the Protein Data Bank, www.pdb.org (PDB ID codes 2R2R, 2R2S, 2R2T, and 2R2U).

‡To whom correspondence may be addressed. E-mail: mgeorgia@iupui.edu or long@chem.iupui.edu.

This article contains supporting information online at www.pnas.org/cgi/content/full/0708143105/DCSupplemental

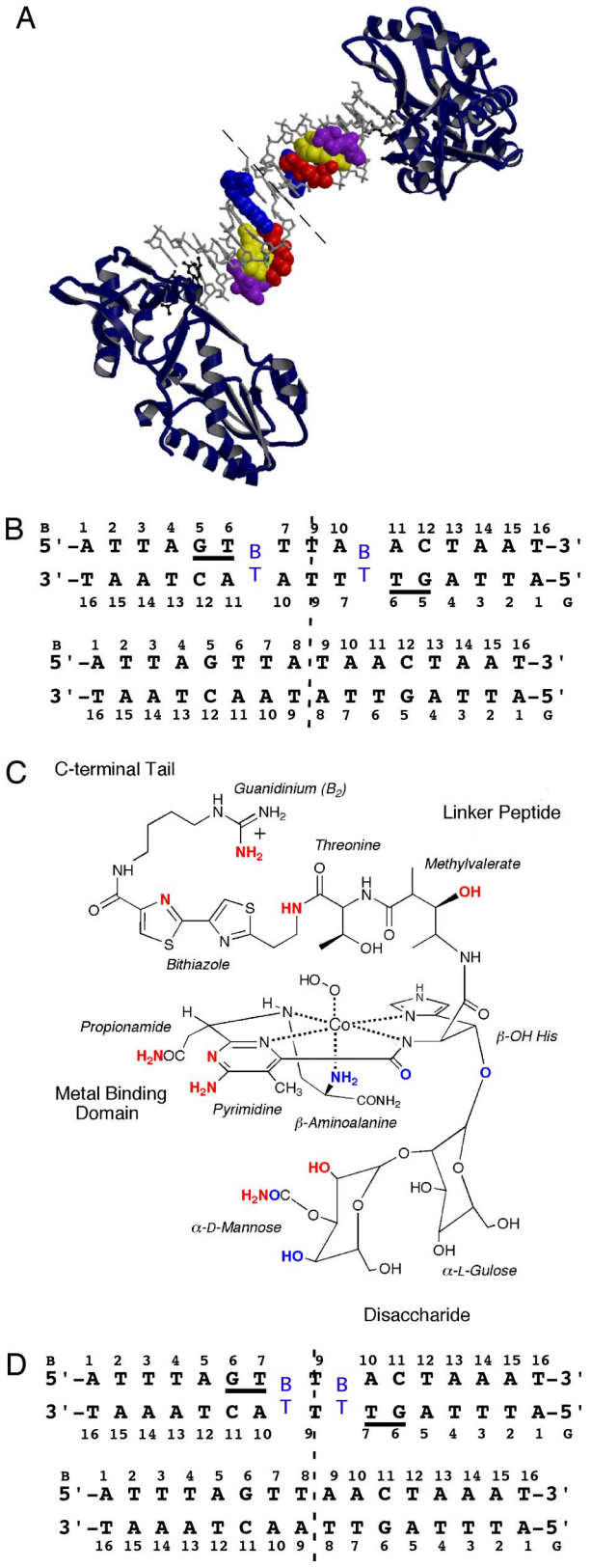

Fig. 1. Overview of the Co·BLM-DNA complex. (*A*) The crystal structure of the RT-DNA-Co·BLM complex. The asymmetric unit consists of one RT molecule, a 7.5-bp oligonucleotide duplex, and one Co·BLM molecule representing half of the symmetric complex. The dashed line represents the dyad. The DNA oligonucleotide is shown in a gray stick model, Co·BLM in CPK with domains color-coded (blue, bithiazole tail; red, threonine-methylvalerate linker; yellow, metal-binding domain with Co in green; purple, disaccharide) and RT as a ribbon rendering in blue. RT residues Asp-114, Leu-115, Arg-116, and Lys-120 make contacts with the DNA and are shown in black ball-and-stick models. (*B*) Schematic of **1** in the presence (*Upper*) and absence (*Bottom*) of Co·BLM with the two complementary strands (B and G) and the numbering scheme referred to in the text. BT, intercalated bithiazole. (*C*) Schematic of HOO-Co(III)·bleomycin B_2. Atoms involved in H-bonding to the DNA are in red, and atoms involved in intramolecular H-bonding are in blue. (*D*) Same as in *B* for **2**.

width at the intercalation site and 5′ GT recognition site are the most significant structural differences; otherwise, the overall structures of bound and unbound DNA are fairly similar despite the formation of the T-T base pair at the dyad (Fig. 3). The first 6 bp of **1**, including the 5′-GT site (A_1-T_6/T_6-A_{11}) in the presence and absence of Co·BLM have an rmsd of 0.60 Å, whereas that of the 5′-GT site (G_5-T_6/A_{11}-C_{12}) alone is 0.58 Å (Fig. 3) (see *SI Text* for information regarding changes in the local structure of the DNA).

Bithiazole Intercalation and Linker. Comparison of the Co·BLM-bound DNA structures revealed two distinct modes of bithiazole intercalation (Fig. 4 *A* and *B*). When bound to **1**, the bithiazole is positioned with its C-terminal thiazole ring stacked between A_{10} and A_{11} (Fig. 1*B*) and the N-terminal thiazole ring occupying a more central position between the base pairs. This binding mode is stabilized by a water-mediated interaction between the C-terminal thiazole ring N (2.9 Å) and the DNA backbone O4′ of A_{11} (2.9 Å) and another water-mediated interaction between the guanidium NH_2 and the N7 of A_{10} that serves to anchor the C-terminal tail within the major groove [NH_2···H_2O···N7 of A_{10} (2.6 Å/3.3 Å)] (Fig. 4*A*; see Table S2 for a complete listing of hydrogen bonding interactions). For the second binding mode observed in **2**, the C-terminal thiazole ring is positioned similarly to that of the N-terminal thiazole ring in **1**, and its N-terminal ring is stacked between T_7 and T_9. The carbonyl of the amide linkage within the C-terminal tail in **2** has an equivalent position to the bridging water molecule in **1** (Fig. 4*B*) and may be important for base stacking on either side of the bithiazole. Thus, in **2**, the C-terminal tail is not "fixed" by hydrogen bonds in the major groove of DNA, because part of the tail is intercalated between the base pairs.

In **1**, the position of the fully intercalated bithiazole is equivalent to one base pair step within the DNA, whereas that in **2** is ≈0.5 Å shorter (**1**: T_6-A_{11} rise was 5.99 Å; **2**: T_7-A_{10} rise was 5.48 Å). Adjustments in rise upon intercalation are concurrent with DNA unwinding of the helix 3′ to the 5′-GT recognition site. The helix of **1** is unwound at the intercalation site by 8.9° (helical twist of T_6-A_{11} step in unbound 36.0° vs. bound 27.1°), whereas the equivalent site in **2** is unwound by only 4.7° (helical twist of T_7-A_{10} step in unbound 33.1° vs. bound 28.4°).

For the binding mode observed in **1**, the linker moiety of Co·BLM is well ordered and makes specific hydrogen-bonding interactions with the sugar–phosphate backbone (Fig. 4*A*). These interactions include the methyl valerate −OH to the O3′ of T_6 (2.8 Å) and the bithiazole NH (amide linkage to Thr) to the O4′ of T_7 (3.2 Å) (Fig. 4*A*). No specific interactions were observed between the DNA and the β-OH of Thr.

Metal-Binding Domain and Disaccharide. A distorted square pyramidal arrangement for the metal binding domain is observed in **1** with the imidazole, deprotonated His amide, pyrimidine N1, and the secondary amine of the β-aminoalanine bound as equatorial ligands and the primary amine as an axial ligand to Co(III) (Fig. 5 and Table S3). Another proposed ligand, the α-D-mannose carbamoyl amide (25), is 6.2 Å from the Co(III) and interacts with the minor groove of the DNA in our structure. No electron density was observed for the hydroperoxide ligand. Although the bithiazole is well ordered with an average B-factor

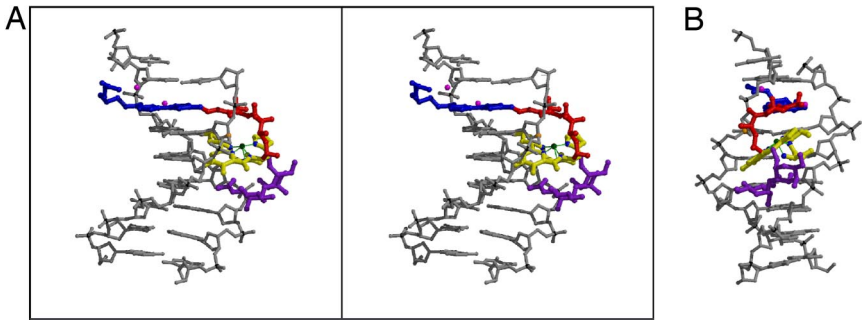

Fig. 2. Structure of the DNA-Co·BLM complex. (*A*) A ball-and-stick stereodiagram rendering is shown with DNA in gray, P atoms are shown in black, and the C4′ of T_6 is shown in orange. Co·BLM domains are color-coded as in Fig. 1*A*. (*B*) Minor groove view of the same complex as in *A*.

of 51.6 Å^2, similar in magnitude to that of the DNA, 51.7 Å^2, the B-factors of the remaining domains of Co·BLM, which have more limited interactions with the DNA, are higher. The linker has an average B-factor of 79.7 Å^2, 1.5-fold that of the bithiazole, and the metal binding domain and disaccharide, although still ordered, have average B-factors of 92.4 Å^2 and 94.5 Å^2, respectively, nearly double those of the bithiazole. The B-factors of the metal-binding and disaccharide domains are consistent with movement of these domains within the minor groove. Thus, the hydroperoxide ligand, which extends from the side of the metal-binding domain, would be expected to have an even higher average B-factor than that of the metal-binding/disaccharide domain and as a consequence ill defined electron density, consistent with our results.

When bound to **1**, the metal-binding domain and disaccharide moieties partially stack against each other and display base-specific hydrogen bonding to each respective wall of the minor groove (Fig. 5 and Table S2): pyrimidine N3 to N2 of G_5 (3.1 Å), the pyrimidine C4-NH_2 to N3 of G_5 (2.4 Å), and the α-D-mannose carbamoyl NH_2 to O2 of T_{13} (2.8 Å). Contacts with the sugar–phosphate backbone include pyrimidine C4-NH_2 to O4′ of G_5 (2.8 Å) and the α-D-mannose C2-OH to O3′ of A_{14} (2.5 Å). Intramolecular hydrogen bonds within DNA-bound Co·BLM (Fig. 5) include the α-D-mannose carbamoyl carbonyl to the NH_2 of β-aminoalanine (3.1 Å), the α-D-mannose C4-OH to the carbonyl of the pyrimidine moiety (2.8 Å), and the β-aminoalanine NH_2 to the β-O of His (3.4 Å). Together, the interactions of the metal-binding domain and disaccharide with the minor groove bury a surface area of 818 Å^2, whereas the interaction between the α-D-mannose moiety, and the metal-binding domain buries 295 Å^2. Based on coordination constraints and comparison with NMR-derived structural models (23, 24), a model of the hydroperoxide ligand places the distal oxygen 2.5 Å from the C4′ atom of T_6 and the coordinating oxygen 4.7 Å from the same C4′ atom (Fig. 5); this finding is entirely consistent with the observations published in refs. 21, 23, and 24.

Discussion

Despite study over the past 40 years, important aspects of the structural organization of metallobleomycin and its interactions with DNA have yet to be resolved. The mode of interaction of the bithiazole with DNA, i.e., minor groove binding (31, 32) vs. full intercalation and/or partial intercalation, has been the subject of debate. In our studies, we find no evidence of minor groove binding by the bithiazole. Rather, we observed two distinct modes of full

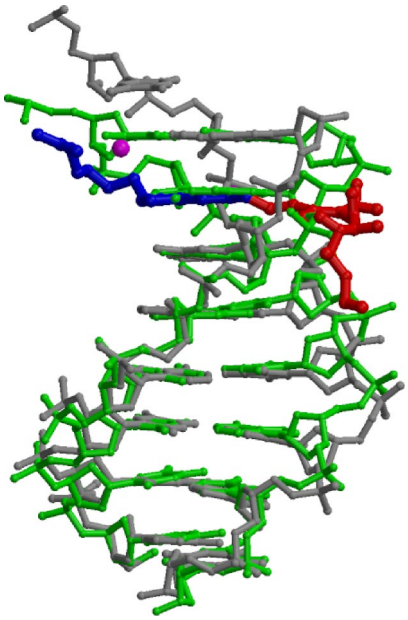

Fig. 3. Comparison of DNA structures with and without Co·BLM. DNA with Co·BLM bound (gray) superimposed on DNA in the absence of Co·BLM (green), showing only the bithiazole/C-terminal tail (blue) and linker (red) of the drug and waters (magenta) (superimposed in O based on C1′ atoms of the first 6 bp, rmsd = 0.60 Å).

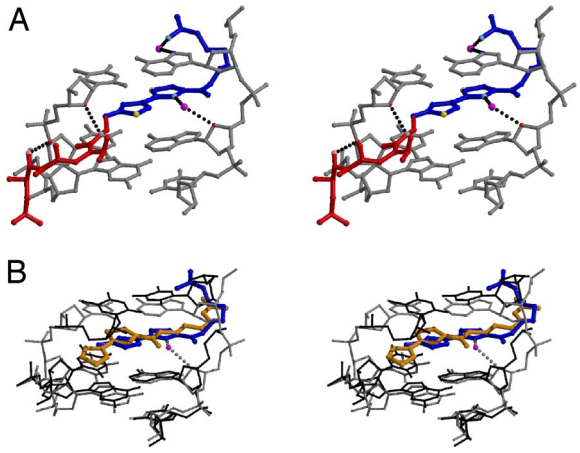

Fig. 4. Interactions of the bithiazole/C-terminal tail and linker with the DNA. (*A*) Stereodiagram of **1** with DNA (gray) and intercalated bithiazole/C-terminal tail (blue) and linker (red) as a ball-and-stick model with waters (magenta) that contribute to bithiazole/C-terminal tail positioning. Hydrogen bonds represented as black dashed lines. Oxygen atoms in red (DNA) or pink (BLM) and nitrogen atoms in blue (DNA) or cyan (Co·BLM) are involved in H-bonding. Sulfur atoms are yellow. (*B*) Superimposed **1** (gray) and **2** (black) 5′-**GT**T sites with intercalated bithiazole/C-terminal tails (**1**, blue; **2**, orange) and relevant water from **1** (magenta) (rmsd of 5′-GT base pairs = 0.54 Å).

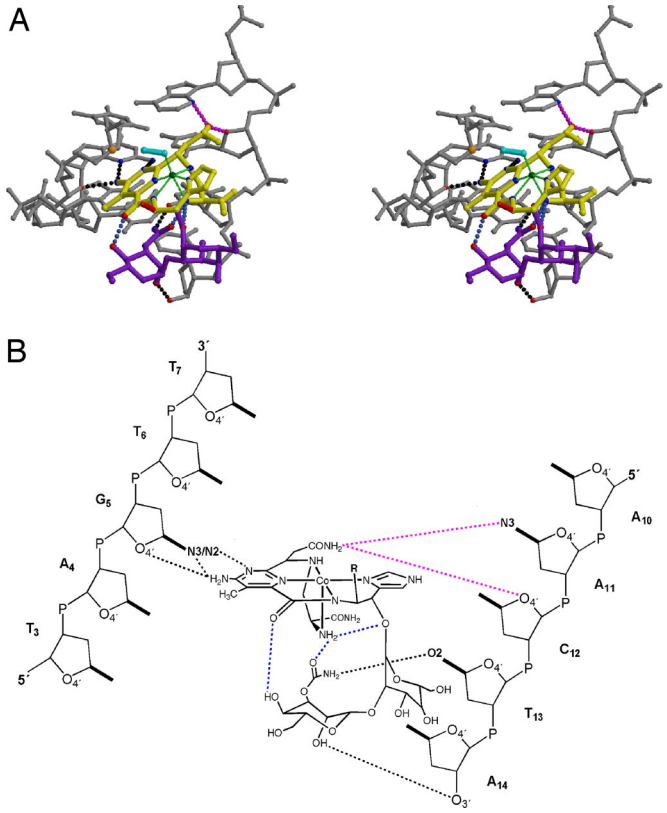

Fig. 5. Interactions of the metal-binding domain and disaccharide with the DNA. (*A*) Stereodiagram of the minor groove of DNA (gray) shown with the metal-binding (yellow with Co in green) and disaccharide (purple) domains and a modeled peroxide ligand (cyan) as a ball-and-stick model. Hydrogen bonds are represented as dashed lines with interacting O atoms in red and N atoms in blue. Intermolecular bonds are black, intramolecular bonds are blue, and magenta bonds represent interactions of the propionamide as modeled (the propioanamide is absent in electron density). The red stick indicates the connection to the linker domain. (*B*) Schematic showing the hydrogen-bonding interactions of the metal-binding and disaccharide domains in the minor groove with bonds colored as in *A*.

intercalation for the bithiazole at the site directly 3′ to the 5′-GT recognition site. In addition, we find that bithiazole intercalation occurs independently of well ordered binding of the metal-binding domain in the minor groove as in **2**.

In 2D NMR-based models, hydrogen-bonding interactions between the Thr-NH and methylvalerate-NH of the linker and the penultimate oxygen of the metal-bound peroxide have been proposed to play an important role in preorganizing the structure of HOO-Co(III)·bleomycin (21, 23, 24). However, these same linker amides in our structure point away from the penultimate oxygen of the hydroperoxide and are therefore not positioned to hydrogen bond to the hydroperoxide ligand (Fig. S1, Fig. S2, and Fig. S3). Instead, the methylvalerate OH and the bithiazole NH hydrogen bond to the DNA (Fig. 4*A*). Our findings indicate that interactions between the linker and the DNA rather than interactions of the linker with the hydroperoxide ligand stabilize the binding of HOO-Co(III)·bleomycin. Intramolecular hydrogen-bonding interactions within HOO-Co(III)·bleomycin discussed above also differ from those observed in the previously reported NMR structures.

The metal-coordinating ligands and screw sense within the metal-binding domain of bleomycin have long been a source of debate (33). The screw sense and Co(III)-coordinating atoms observed in our structure are the same as those proposed in the NMR structures of HOO-Co(III)·bleomycin bound to DNA (21, 23, 24), although the structures clearly differ in detail (Figs. S1–S3). More recently, the primary amine of β-aminoalanine has been identified definitively as an axial ligand to Co(III) (34) consistent with earlier models (21, 23, 24).

In NMR derived models, neither the α-D-mannose nor the gulopyranose make direct contacts with the DNA (21, 23, 24). In our structure, no interactions were observed between the gulopyanose moiety and the DNA, but the α-D-mannose carbamoyl NH_2 hydrogen-bonds to the O_2 of T_{13} in the minor groove. Thus, no functional role for the gulopyranose can be assigned based on structural analysis. Nonetheless, an important role for the disaccharide moiety in DNA-binding and cleavage by HOO-Fe(III)·bleomycin has been indicated by the reduced DNA cleavage activity of deglycobleomycin *in vitro* (35, 36). One possibility is that the gulopyranose serves as a "space-filling" unit allowing the metal binding domain to adopt an optimized and stabilized orientation relative to the target C4′-H. We further note that the respective orientations and intramolecular hydrogen-bonding interactions of the metal-binding and disaccharide domains of Co·BLM bound to **1** are similar to those observed in the crystal structure of Cu(II)·bleomycin bound to a bleomycin resistance protein (37) (Fig. S1). This finding suggests that binding of bleomycin to a protein or DNA inherently favors partial stacking of the metal binding domain and disaccharide moieties facilitated by intramolecular hydrogen bonding interactions.

The interactions described above all serve to bring the reactive metal center of metallobleomycin into close proximity to a target C4′-H. Recent experimental and theoretical studies suggest that HOO-Fe(III)·bleomycin induces single strand DNA breaks through abstraction of the C4′-H with concerted cleavage of the O—O bond (38). Based on our structural analysis, we propose that HOO-Fe(III)·bleomycin adopts a similar structural arrangement to that found in our model of HOO-Co(III)·bleomycin bound to DNA facilitating abstraction of the C4′-H by the distal oxygen of the hydroperoxide, which is appropriately positioned in our model to effect this chemistry.

Methods

Crystallization. The RT fragment (residues 24–278) (29) and DNA oligonucleotides were purified and RT-DNA crystals were grown as described in ref. 27. Co·BLM was prepared from bleomycin B_2 (Calbiochem), metallated as described in refs. 21 and 39, purified by HPLC, and verified by LC-MS. For Co·BLM soaks, crystals were soaked in well solutions containing 0.1 mM Co·BLM followed by stabilization in 9% PEG 4000, 5 mM magnesium acetate, 100 mM Hepes (pH 8.0), and 20% ethylene glycol containing 0.25 mM Co·BLM until unit cell changes were detected.

Data Collection and Refinement. Data were collected at beamline 19-ID of the Advanced Photon Source and integrated and processed with the HKL2000 package (40). Crystal structures were determined by molecular replacement with AMoRe (41), using the refined model of the N-terminal fragment of MMLV RT as the search model (PDB ID code 1ZTW) to obtain unbiased electron density of the DNA and drug. Coordinates for the B-form model of the desired DNA sequence were generated by using Nucleic Acid Builder (42) and adjusted manually to fit the electron density, using O (43). After addition of water molecules, Co·BLM was modeled into the density map starting with a composite model of the drug obtained from 2D NMR (24) and crystallographic data (32). Our initial F_o-F_c map displayed good density for the intercalated bithiazole domain and metal-binding domain and some density for the disaccharide (Fig. S4). The drug was modeled in parts starting with the bithiazole domain and C-terminal tail, followed by the metal-binding domain, the Thr-methylvalerate linker region to connect the two, and further addition of the disaccharide. A *trans* conformation of the bithiazole moiety was confirmed in the difference maps. Alternate cycles of model building, using O (43), and refinement calculations in CNS (44) were completed until no large peaks remained in the F_o-F_c electron density maps. The final Co·BLM model was verified by using SA omit map analysis (44). A summary of the refinement statistics is shown in Table S1. DNA structural parameters were analyzed by using 3DNA (45). Surface area calculations were performed by using NACCESS

(46). Figures were generated by using MOLSCRIPT (47) and RASTER 3D (48, 49). Coordinates for the hydroperoxide model are available upon request.

ACKNOWLEDGMENTS. We thank Marianne Cuff, Steve Ginell, and Andrzej Joachimiak from the Structural Biology Center Collaborative Access Team at the Advanced Photon Source. Results shown in this report are derived from work performed at Argonne National Laboratory, Structural Biology Center at the Advanced Photon Source. Argonne is operated by UChicago Argonne, LLC, for the U.S. Department of Energy, Office of Biological and Environmental Research under Contract DE-AC02-06CH11357. This work was supported by a fellowship from the American Cancer Society (to K.D.G.) and the National Institutes of Health (E.C.L. and M.M.G.).

1. Umezawa H, Maeda K, Takeuchi T, Okami Y (1966) New antibiotics, bleomycin A and B. *J Antibiot (Tokyo)* 19:200–209.
2. Connors JM (2005) State-of-the-art therapeutics: Hodgkin's lymphoma. *J Clin Oncol* 23:6400–6408.
3. Reyes F, *et al.* (2005) ACVBP versus CHOP plus radiotherapy for localized aggressive lymphoma. *N Engl J Med* 352:1197–1205.
4. Einhorn LH (2002) Curing metastatic testicular cancer. *Proc Natl Acad Sci USA* 99:4592–4595.
5. Nagai K, *et al.* (1969) The combined effects of bleomycin and sulfhydryl compounds on the thermal denaturation of DNA. *Biochim Biophys Acta* 179:165–171.
6. Povirk LF, Wubker W, Kohnlein W, Hutchinson F (1977) DNA double-strand breaks and alkali-labile bonds produced by bleomycin. *Nucleic Acids Res* 4:3573–3579.
7. Sausville EA, Peisach J, Horwitz SB (1976) A role for ferrous ion and oxygen in the degradation of DNA by bleomycin. *Biochem Biophys Res Commun* 73:814–822.
8. Wu JC, Kozarich JW, Stubbe J (1985) Mechanism of bleomycin: Evidence for a rate-determining 4′-hydrogen abstraction from poly(dA-dU) associated with the formation of both free base and base propenal. *Biochemistry* 24:7562–7568.
9. D'Andrea AD, Haseltine WA (1978) Sequence specific cleavage of DNA by the antitumor antibiotics neocarzinostatin and bleomycin. *Proc Natl Acad Sci USA* 75:3608–3612.
10. Carter BJ, *et al.* (1990) Site-specific cleavage of RNA by Fe(II)·bleomycin. *Proc Natl Acad Sci USA* 87:9373–9377.
11. Ehrenfeld GM, *et al.* (1987) Copper-dependent cleavage of DNA by bleomycin. *Biochemistry* 26:931–942.
12. Hecht SM (2005) in *Anticancer Agents from Natural Products*, eds Cragg GM, Kingston DGI, Newman DJ (CRC, Boca Raton, FL), pp 357–381.
13. Boger DL, Cai H (1999) Bleomycin: Synthetic and mechanistic studies. *Angew Chem Int Ed* 38:448–476.
14. Chen J, Stubbe J (2005) Bleomycins: Towards better therapeutics. *Nat Rev Cancer* 5:102–112.
15. Chang CH, Dallas JL, Meares CF (1983) Identification of a key structural feature of cobalt(III)-bleomycins: An exogenous ligand (e.g. hydroperoxide) bound to cobalt. *Biochem Biophys Res Commun* 110:959–966.
16. Chang CH, Meares CF (1982) Light-induced nicking of deoxyribonucleic acid by cobalt(III) bleomycins. *Biochemistry* 21:6332–6334.
17. Nightingale KP, Fox KR (1993) DNA structure influences sequence specific cleavage by bleomycin. *Nucleic Acids Res* 21:2549–2555.
18. Nightingale KP, Fox KR (1994) Light-activated cleavage of DNA by cobalt-bleomycin. *Eur J Biochem* 220:173–181.
19. McLean MJ, Dar A, Waring MJ (1989) Differences between sites of binding to DNA and strand cleavage for complexes of bleomycin with iron or cobalt. *J Mol Recognit* 1:184–192.
20. Lewis MA, Long EC (2006) Fluorescent intercalator displacement analyses of DNA binding by the peptide-derived natural products netropsin, actinomycin, and bleomycin. *Bioorg Med Chem* 14:3481–3490.
21. Wu W, *et al.* (1996) Solution structure of Co·bleomycin A2 green complexed with $d(CCAGGCCTGG)_2$. *J Am Chem Soc* 118:1281–1294.
22. Vanderwall DE, *et al.* (1997) A model of the structure of HOO-Co·bleomycin bound to $d(CCAGTACTGG)_2$: Recognition at the d(GpT) site and implications for double-stranded DNA cleavage. *Chem Biol* 4:373–387.
23. Zhao C, *et al.* (2002) Structures of HO_2-Co(III)bleomycin A_2 bound to $d(GAGCTC)_2$ and $d(GGAAGCTTCC)_2$: Structure-reactivity relationships of Co and Fe bleomycins. *J Inorg Biochem* 91:259–268.
24. Hoehn ST, *et al.* (2001) Solution structure of Co(III)-bleomycin-OOH bound to a phosphoglycolate lesion containing oligonucleotide: Implications for bleomycin-induced double-strand DNA cleavage. *Biochemistry* 40:5894–5905.
25. Stubbe J, Kozarich JW (1987) Mechanisms of bleomycin-induced DNA degradation. *Chem Rev* 87:1107–1136.
26. Goodwin KD, Long EC, Georgiadis MM (2005) A host-guest approach for determining drug-DNA interactions: An example using netropsin. *Nucleic Acids Res* 33:4106–4116.
27. Goodwin KD, *et al.* (2006) A high-throughput, high-resolution strategy for the study of site-selective DNA binding agents: Analysis of a ''highly twisted'' benzimidazole-diamidine. *J Am Chem Soc* 128:7846–7854.
28. Cote, ML, Yohannan, SJ, Georgiadis, MM (2000) Use of an N-terminal fragment from moloney murine leukemia virus reverse transcriptase to facilitate crystallization and analysis of a pseudo-16-mer DNA molecule containing G-A mispairs. *Acta Crystallogr D* 56 (Pt 9):1120–1131.
29. Sun D, *et al.* (1998) Cloning, expression, and purification of a catalytic fragment of Moloney murine leukemia virus reverse transcriptase: Crystallization of nucleic acid complexes. *Protein Sci* 7:1575–1582.
30. Parker JB, *et al.* (2007) Enzymatic capture of an extrahelical thymine in the search for uracil in DNA. *Nature* 449:433–437.
31. Kuwahara J, Sugiura Y (1988) Sequence-specific recognition and cleavage of DNA by metallobleomycin: Minor groove binding and possible interaction mode. *Proc Natl Acad Sci USA* 85:2459–2463.
32. Manderville RA, Ellena JF, Hecht SM (1994) Solution structure of a Zn(II)-bleomycin A_5-$d(CGCTAGCG)_2$ complex. *J Am Chem Soc* 116:10851–10852.
33. Claussen CA, Long EC (1999) Nucleic Acid recognition by metal complexes of bleomycin. *Chem Rev* 99:2797–2816.
34. Xia C, Forsterling FH, Petering DH (2003) Identification of the internal axial ligand of HO_2-cobalt(III)-bleomycin: $^1H[^{15}N]$ HSQC NMR investigation of bleomycin, deglycobleomycin, and their hydroperoxide-cobalt(III) complexes. *Biochemistry* 42:6559–6564.
35. Oppenheimer NJ, *et al.* (1982) Deglyco-bleomycin. Degradation of DNA and formation of a structurally unique Fe(II)·CO complex. *J Biol Chem* 257:1606–1609.
36. Sugiyama H, *et al.* (1985) DNA strand scission by bleomycin group antibiotics. *J Nat Prod* 48:869–877.
37. Sugiyama M, *et al.* (2002) The 1.6-Å crystal structure of the copper(II)-bound bleomycin complexed with the bleomycin-binding protein from bleomycin-producing Streptomyces verticillus. *J Biol Chem* 277:2311–2320.
38. Decker A, *et al.* (2006) Direct hydrogen-atom abstraction by activated bleomycin: An experimental and computational study. *J Am Chem Soc* 128:4719–4733.
39. Rajani C, Kincaid JR, Petering DH (2004) Resonance Raman studies of HOO-Co(III)bleomycin and Co(III)bleomycin: Identification of two important vibrational modes, ν(Co-OOH) and ν (O-OH). *J Am Chem Soc* 126:3829–3836.
40. Otwinowski Z, Minor W (1997) in *Macromolecular Crystallography, Part A*, eds Carter CW, Jr, Sweet RM (Academic, New York), Vol 276, pp 307–326.
41. Navaza J (1994) AMoRe: An automated package for molecular replacement. *Acta Crystallogr A* 50:157–163.
42. Macke T, Case DA (1998) in *Molecular Modeling of Nucleic Acids*, eds Leontes NB, SantaLucia J, Jr (American Chemical Society, Washington, DC), Vol. 1, pp 379–393.
43. Jones TA, Zou JY, Cowan SW, Kjeldgaard M (1991) Improved methods for building protein models in electron density maps and the location of errors in these models. *Acta Crystallogr A* 47:110–119.
44. Brunger, AT, *et al.* (1998) Crystallography & NMR system: A new software suite for macromolecular structure determination. *Acta Crystallogr D* 54 (Pt 5):905–921.
45. Lu XJ, Olson WK (2003) 3DNA: A software package for the analysis, rebuilding and visualization of three-dimensional nucleic acid structures. *Nucleic Acids Res* 31:5108–5121.
46. Hubbard SJ, Thornton JM (1993) *NACCESS* (University College London, London).
47. Kraulis PJ (1991) MOLSCRIPT: A Program to produce both detailed and schematic plots of protein structures. *J Appl Cryst* 24:946–950.
48. Merritt EA, Murphy MEP (1994) Raster3D Version 2.0—A program for photorealistic molecular graphics. *Acta Crystallogr D* 50:869–873.
49. Bacon DJ, Anderson WF (1988) A fast algorithm for rendering space-filling molecule pictures. *J Mol Graphics* 6:219–220.